Prepared for submission to JHEP

arXiv:1612.05059v1 [hep-lat] 15 Dec 2016

Localisation and chiral properties near the ordering transition of an Anderson-like toy model for QCD

Matteo Giordano[a], **Tamás G. Kovács**[b], **and Ferenc Pittler**[c]

[a] *MTA-ELTE Lattice Gauge Theory Research Group, Pázmány P. sétány 1/A, H-1117 Budapest, Hungary*

[b] *Institute for Nuclear Research of the Hungarian Academy of Sciences, Bem tér 18/c, H-4026 Debrecen, Hungary*

[c] *HISKP(Theory), University of Bonn, Nussallee 14-16, D-53115 Bonn, Germany*

E-mail: giordano@bodri.elte.hu, kgt@atomki.mta.hu, pittler@hiskp.uni-bonn.de

Abstract: The Dirac operator in finite temperature QCD is equivalent to the Hamiltonian of an unconventional Anderson model, with on-site noise provided by the fluctuations of the Polyakov lines. The main features of its spectrum and eigenvectors, concerning the density of low modes and their localisation properties, are qualitatively reproduced by a toy-model random Hamiltonian, based on an Ising-type spin model mimicking the dynamics of the Polyakov lines. Here we study the low modes of this toy model in the vicinity of the ordering transition of the spin model, and show that at the critical point the spectral density at the origin has a singularity, and the localisation properties of the lowest modes change. This provides further evidence of the close relation between deconfinement, chiral transition and localisation of the low modes.

Keywords: Lattice QCD, Phase Diagram of QCD, Random Systems

Contents

1 Introduction **1**

2 The Dirac operator as an Anderson-like Hamiltonian **3**
- 2.1 Simplifications of the Dirac-Anderson Hamiltonian 5
- 2.2 Dirac-Anderson Hamiltonian for $N_T = N_c = 2$ 8
- 2.3 Toy model 8

3 Numerical results **10**
- 3.1 Finite-size-scaling study of the spin model 11
- 3.2 Onset of localisation and chiral transition in the toy model 13

4 Conclusions and outlook **17**

1 Introduction

As is well known, the phase diagram of QCD at zero chemical potential consists of a low-temperature confining and chirally-broken phase, and a high-temperature deconfined and (approximately) chirally-restored phase. Interestingly enough, the two transitions take place at nearly the same temperature, or more precisely in the same small temperature range, as both the deconfining and the chirally-restoring transition are actually steep but nevertheless analytic crossovers [1, 2]. The close connection between the two transitions is even more striking in certain QCD-like models where they are genuine phase transitions, like for example SU(2) and SU(3) pure-gauge theories. In this case lattice calculations show that the deconfinement and the chiral transitions take place at the very same temperature (of course, within the inherent numerical uncertainties of lattice calculations) [3]. The same coincidence of the transition temperatures has been observed in a model with SU(3) gauge fields and unimproved staggered fermions on coarse lattices [4–6]. Another interesting case is that of SU(3) gauge fields with adjoint fermions: this model is known to possess different deconfinement (T_d) and chiral-restoration temperatures (T_χ) [7], with $T_d < T_\chi$, but the chiral condensate has a jump exactly at T_d, signalling a first-order chiral phase transition there. So far, no generally accepted explanation has been provided for the coincidence of chiral and deconfinement transitions in these models, and their approximate coincidence in QCD.

In recent years there has been growing evidence that the QCD finite-temperature transition is accompanied by a change in the localisation properties of the Dirac eigenmodes: while in the low-temperature phase all the Dirac eigenmodes are delocalised in the whole volume [8, 9], at high temperature the lowest modes are spatially localised [10–21]. This

behaviour of the lowest modes is not unique to QCD, and has been found also in the above-mentioned QCD-like models (i.e., SU(2) and SU(3) pure gauge theory, and unimproved staggered fermions). There are indications that the onset of localisation takes place around the same temperature at which QCD becomes deconfined and chirally restored: this issue was first studied by Osborn and García-García in Ref. [11]. To avoid the complications related to the crossover nature of the QCD transition, it is convenient to consider models where the transition is a genuine phase transition. This was done in Ref. [18], which employed the above-mentioned model with unimproved staggered fermions, investigating the confining, chiral and localisation properties of the system. In that case, it was found that deconfinement, (approximate) chiral restoration, and onset of localisation take place at the same value of the gauge coupling, where the system undergoes a first-order phase transition. These results obviously suggest that localisation is closely related to deconfinement and to the chiral transition.

Understanding why the lowest Dirac eigenmodes become localised at the transition, and how localisation affects the corresponding eigenvalues, might help in shedding some light on the relation between the deconfining and the chiral transition. As it was suggested in Ref. [14], and later elaborated on in more detail in Refs. [22, 23], localisation of the lowest modes is very likely to be a consequence of deconfinement. More precisely, the ordering of the Polyakov-line configurations, and the presence therein of "islands" of fluctuations away from the ordered value, leads to the lowest Dirac modes localising on the "islands". In Ref. [23] it was suggested that the ordering of the Polyakov lines might also be responsible for the depletion of the spectral region near the origin, which in turn leads to a smaller condensate via the Banks-Casher relation, and so to approximate chiral restoration.

The argument is most clearly formulated in the Dirac-Anderson approach of Ref. [23]. This consists in recasting the Dirac operator into the Hamiltonian of a three-dimensional system with internal degrees of freedom, corresponding to colour and temporal momentum. This Hamiltonian contains a diagonal part, related to the phases of the Polyakov lines, representing a random on-site potential for the quarks, and an off-diagonal part responsible for their hopping from site to site, built out of the spatial links on the different time slices. In this framework, the accumulation of eigenmodes near the origin requires two conditions: sufficiently many sites where the on-site potential is small, and a sufficiently strong mixing (via the hopping terms) of the different temporal-momentum components of the quark wave function. The ordering of the Polyakov lines acts against both these requirements, by reducing the number of sites where the potential is small, and localising them on "islands" in a "sea" of sites where the potential is large; and by inducing correlations among spatial links on different time slices, which in turn makes the mixing of different temporal-momentum components less effective. This leads to the depletion of the spectral region near the origin.

The argument above is based on the results of a detailed numerical study of a QCD-inspired toy model, constructed in such a way as to reproduce qualitatively all the important features of the QCD Dirac spectrum and of the corresponding eigenmodes. In this toy model the role of the Polyakov lines is played by complex spin variables, with dynamics determined by an Ising-like model. This spin model possesses a disordered and an ordered phase, analo-

gous to the confined and deconfined phases of gauge theories. As was shown in Ref. [23], the properties of the Dirac spectrum in the ordered and disordered phases indeed qualitatively match those found in the deconfined and confined phases of QCD, respectively. More precisely, deep in the ordered phase the lowest eigenmodes are localised and the spectral density vanishes near the origin, while in the disordered phase the lowest eigenmodes are delocalised and the spectral density is finite near the origin. This makes us confident in the validity of the mechanism for chiral symmetry restoration discussed above also in the physically relevant case of QCD.

The magnetisation transition of the spin model is expected to be in the same universality class as that of the 3D Ising model, so one expects it to be a genuine second-order phase transition. It is thus worth studying the localisation properties of the lowest Dirac eigenmodes, and the corresponding spectral density near the origin, close to the magnetisation transition. This is the subject of the present paper. The purpose is twofold: on the one hand, this model provides another testing ground for the idea that deconfinement, chiral transition and localisation of the lowest modes are closely connected. On the other hand, the different order of the transition with respect to that taking place in the model with unimproved staggered fermions allows us to study the possible dependence of this connection on the nature of the transition.

The paper is organised as follows. In Section 2 we review the approach to the QCD Dirac spectrum as the spectrum of a Hamiltonian with noise ("Dirac-Anderson" approach), considerably simplifying the formalism of Ref. [23]. We then briefly recall the main aspects of the toy model of Ref. [23], which we reformulate equivalently in the new formalism. In Section 3 we show our numerical results. We first identify precisely the critical point of the spin model, and then discuss the localisation and chiral properties of our toy model in its vicinity. Finally, in Section 4 we report our conclusions and show our prospects for the future.

2 The Dirac operator as an Anderson-like Hamiltonian

In this section we briefly review the derivation of the Dirac-Anderson form of the staggered Dirac operator, introduced in Ref. [23]. We also proceed to simplify the formalism with respect to the original formulation.

The Dirac-Anderson Hamiltonian is nothing but a suggestive name for (minus i times) the staggered Dirac operator in the basis of the eigenvectors of the temporal hopping term. More precisely, denoting it by $\mathcal{H} = -iD_{\text{stag}}$, it reads in compact notation

$$\mathcal{H} = \eta_4 \mathcal{D} + \frac{1}{2i} \sum_{j=1}^{3} \eta_j \left[\mathcal{V}_j \mathcal{T}_j - \mathcal{T}_j^\dagger \mathcal{V}_j^\dagger \right] . \tag{2.1}$$

The Dirac-Anderson Hamiltonian, $\mathcal{H}_{\vec{x}ak,\vec{y}bl}$, carries space, colour and temporal-momentum indices, for $\vec{x},\vec{y} \in \mathbb{Z}_L^3$, $a,b = 1,\ldots,N_c$, and $k,l = 0,\ldots,N_T-1$. Here $\mathbb{Z}_L^3 = \{\vec{x}\,|\,0 \leq x_i \leq L-1\}$, and L and N_T are the spatial and temporal extension of the lattice, which

have to be even integer numbers. Periodic boundary conditions in the spatial directions are understood.[1] In Eq. (2.1), $\mathcal{D}$ is the diagonal matrix consisting of the "unperturbed" eigenvalues of the temporal hopping term, $\mathcal{V}_j$ come from the spatial hoppings, and $\mathcal{T}_j$ is the translation operator in direction j,

$$\begin{aligned}(\mathcal{D})_{\vec{x}ak,\vec{y}bl} &= \delta_{\vec{x}\vec{y}}\delta_{ab}\delta_{kl}\sin\omega_{ak}(\vec{x})\,,\\ (\mathcal{V}_j)_{\vec{x}ak,\vec{y}bl} &= \delta_{\vec{x}\vec{y}}(V_{+j}(\vec{x}))_{ak,bl}\,,\\ (\mathcal{T}_j)_{\vec{x}ak,\vec{y}bl} &= \delta_{\vec{x}+\hat{\jmath},\vec{y}}\delta_{ab}\delta_{kl}\,,\end{aligned} \tag{2.2}$$

and moreover $\eta_\mu = (-1)^{\sum_{\nu<\mu} x_\nu}$ are the usual staggered phases. Let us explain the notation in detail. The effective Matsubara frequencies $\omega_{ak}(\vec{x})$ are given by

$$\omega_{ak}(\vec{x}) = \frac{\pi + \phi_a(\vec{x}) + 2\pi k}{N_T}\,, \tag{2.3}$$

with $\phi_a(\vec{x})$ the phases of the Polyakov line $P(\vec{x}) = \prod_{t=0}^{N_T-1} U_4(t,\vec{x})$. The following convention is chosen for the Polyakov line phases: $\phi_a(\vec{x}) \in [-\pi,\pi)$ for $a = 1,\ldots,N_c-1$, and $\sum_a \phi_a(\vec{x}) = 0$.[2] The spatial hoppings read

$$(V_{+j}(\vec{x}))_{ak,bl} = \frac{1}{N_T}\sum_{t=0}^{N_T-1} e^{i\frac{2\pi t}{N_T}(l-k)} e^{i\frac{t}{N_T}(\phi_b(\vec{x}+\hat{\jmath})-\phi_a(\vec{x}))} (U_j^{(\mathrm{td})}(t,\vec{x}))_{ab}\,, \tag{2.4}$$

where $U_j^{(\mathrm{td})}(t,\vec{x})$ is the gauge link corresponding to the lattice link $(t,\vec{x}) \to (t,\vec{x}+\hat{\jmath})$ in the temporal diagonal gauge (or Polyakov gauge), $U_4^{(\mathrm{td})}(t,\vec{x}) = \mathbf{1}$ for $0 \le t < N_T - 1$ and $U_4^{(\mathrm{td})}(N_T-1,\vec{x}) = \mathrm{diag}(e^{i\phi_a(\vec{x})})$. One can show that $V_{+j}(\vec{x})$ is a unitary matrix in colour and temporal-momentum space.

The expression Eq. (2.1) is obviously fully equivalent to the staggered Dirac operator. Moreover, its structure is reminiscent of a 3D Anderson Hamiltonian with internal degrees of freedom corresponding to colour and temporal momentum, and with antisymmetric rather than symmetric hopping term. The diagonal noise is provided by the phases of the Polyakov lines. The off-diagonal noise present in the hopping terms comes both from the spatial links and from the Polyakov line phases. The amount of disorder is controlled by the size of the fluctuations of the Polyakov lines and of the spatial links, and therefore by the temperature of the system (as well as the lattice spacing).

Differently from the usual Anderson models, the strength of the disorder is fixed, since the absolute value of the diagonal terms is bounded by 1, and since the hopping terms are unitary matrices. What is different on the two sides of the deconfinement transition is the distribution of the diagonal terms, and the matrix structure of the hoppings. Indeed, at high temperature the ordering of the Polyakov line leads to the enhancement of diagonal terms

[1] Antiperiodic boundary conditions are of course understood in the original staggered operator, but are not needed here.

[2] A redefinition modulo 2π corresponds simply to a unitary transformation of the Hamiltonian [23].

corresponding to the trivial phase $\phi_a(\vec{x}) = 0$, which form a "sea" of large (i.e., close to 1) unperturbed eigenvalues. Fluctuations away from the trivial phase form localised "islands" of smaller unperturbed eigenvalues. Moreover, the ordering of the Polyakov lines leads to strong correlations among spatial links on different time-slices. These correlations tend to reduce the off-diagonal entries of the hopping term in temporal-momentum space in the "sea" region, thus approximately decoupling the different temporal-momentum components of the quark wave-function. At low temperatures, on the other hand, correlations across time-slices are weaker, and the different temporal-momentum components of the quark wave-function mix effectively.

2.1 Simplifications of the Dirac-Anderson Hamiltonian

We now discuss a few convenient simplifications of the Dirac-Anderson Hamiltonian, Eq. (2.1). First of all, by making a suitable gauge transformation we will disentangle the two sources of noise, i.e., we will make the hopping terms independent of the Polyakov line phases. Let us define

$$W(\vec{x}) = \mathrm{diag}\left(e^{i\frac{\phi_a(\vec{x})}{N_T}}\right), \tag{2.5}$$

which satisfies $W(\vec{x})^{N_T} = P(\vec{x})$, and moreover is easily seen to be unitary and unimodular, thanks to our choice of convention for the phases of the Polyakov lines. Eq. (2.4) can then be recast as

$$V_{+j}(\vec{x}) = \frac{1}{N_T}\sum_{t=0}^{N_T-1} e^{i\frac{2\pi t}{N_T}(l-k)}\hat{U}_j(t,\vec{x}), \tag{2.6}$$

where

$$\hat{U}_j(t,\vec{x}) = [W(\vec{x})^\dagger]^t U_j^{(\mathrm{td})}(t,\vec{x})[W(\vec{x}+\hat{\jmath})]^t. \tag{2.7}$$

Since $W(\vec{x}) \in \mathrm{SU}(N_c)$, Eq. (2.7) is just a gauge transformation, that leads to the "uniform diagonal" gauge: since $\hat{U}_4(t,\vec{x}) = [W(\vec{x})^\dagger]^t W(\vec{x})^{t+1} = W(\vec{x})$, one has that the temporal links are constant and diagonal. For future reference, we notice that in this gauge the contribution of time-space plaquettes to the Wilson action, which in the temporal diagonal gauge is proportional to

$$\begin{aligned}\Delta S_{ts} = &\sum_{j,\vec{x}}\sum_{t=0}^{N_T-2}\mathrm{Re}\,\mathrm{tr}\,[U_j^{(\mathrm{td})}(t,\vec{x})U_j^{(\mathrm{td})}(t+1,\vec{x})^\dagger] \\ &+\sum_{j,\vec{x}}\mathrm{Re}\,\mathrm{tr}\,[U_j^{(\mathrm{td})}(N_T-1,\vec{x})P(\vec{x}+\hat{\jmath})U_j^{(\mathrm{td})}(0,\vec{x})^\dagger P(\vec{x})^\dagger],\end{aligned} \tag{2.8}$$

becomes

$$\Delta S_{ts} = \sum_{j,\vec{x}}\sum_{t=0}^{N_T-1}\mathrm{Re}\,\mathrm{tr}\,[\hat{U}_j(t,\vec{x})W(\vec{x}+\hat{\jmath})\hat{U}_j(t+1,\vec{x})^\dagger W(\vec{x})^\dagger]. \tag{2.9}$$

The form of the space-space plaquettes is unaffected by the gauge transformation, and so

$$\begin{aligned}\Delta S_{ss} &= \sum_{j<j',\vec{x},t} \mathrm{Re}\,\mathrm{tr}\,[U_j^{(\mathrm{td})}(t,\vec{x})U_{j'}^{(\mathrm{td})}(t,\vec{x}+\hat{\jmath})U_j^{(\mathrm{td})}(t,\vec{x}+\hat{\jmath}')^\dagger U_{j'}^{(\mathrm{td})}(t,\vec{x})^\dagger] \\ &= \sum_{j<j',\vec{x},t} \mathrm{Re}\,\mathrm{tr}\,[\hat{U}_j(t,\vec{x})\hat{U}_{j'}(t,\vec{x}+\hat{\jmath})\hat{U}_j(t,\vec{x}+\hat{\jmath}')^\dagger \hat{U}_{j'}(t,\vec{x})^\dagger]\,.\end{aligned} \tag{2.10}$$

The second simplification is obtained by using the following property of the diagonal entries,

$$\sin\omega_{a\bar{k}}(\vec{x}) = -\sin\omega_{ak}(\vec{x})\,, \quad \bar{k} \equiv \left(k+\frac{N_T}{2}\right)_{N_T}\,, \tag{2.11}$$

where $(a+b)_{N_T} \equiv a+b \mod N_T$, and the cyclicity of V_{+j}, in particular the property

$$(V_{+j}(\vec{x}))_{ak,bl} = (V_{+j}(\vec{x}))_{a\bar{k},b\bar{l}}\,. \tag{2.12}$$

This allows us to organise the matrices $\mathcal{D}$ and $\mathcal{V}_j$ in blocks of size $\frac{N_T}{2}\times\frac{N_T}{2}$. Explicitly, we can write

$$\mathcal{D} = \begin{pmatrix} \mathscr{D} & \mathbf{0} \\ \mathbf{0} & -\mathscr{D}\end{pmatrix} = \mathscr{D}\Sigma_3\,, \qquad \mathcal{V}_j = \begin{pmatrix} \mathscr{A}_j & \mathscr{B}_j \\ \mathscr{B}_j & \mathscr{A}_j\end{pmatrix} = \mathscr{A}_j + \mathscr{B}_j\Sigma_1\,, \tag{2.13}$$

where

$$\begin{aligned}(\mathscr{D})_{\vec{x}ak,\vec{y}bl} &= \delta_{\vec{x}\vec{y}}\delta_{ab}\delta_{kl}\sin\omega_{ak}(\vec{x})\,, \quad k,l=0,\ldots,\tfrac{N_T}{2}-1\,, \\ (\mathscr{A}_j)_{\vec{x}ak,\vec{y}bl} &= (\mathcal{V}_j)_{\vec{x}ak,\vec{y}bl}\,, \quad (\mathscr{B}_j)_{\vec{x}ak,\vec{y}bl} = (\mathcal{V}_j)_{\vec{x}ak,\vec{y}b\bar{l}}\,, \quad k,l=0,\ldots,\tfrac{N_T}{2}-1\,,\end{aligned} \tag{2.14}$$

and where $\Sigma_i = \sigma_i \otimes \mathbf{1}_{\frac{N_T}{2}}$, i.e.,

$$\Sigma_1 = \begin{pmatrix}\mathbf{0} & \mathbf{1}\\ \mathbf{1} & \mathbf{0}\end{pmatrix}\,, \quad \Sigma_2 = \begin{pmatrix}\mathbf{0} & -i\mathbf{1}\\ i\mathbf{1} & \mathbf{0}\end{pmatrix}\,, \quad \Sigma_3 = \begin{pmatrix}\mathbf{1} & \mathbf{0}\\ \mathbf{0} & -\mathbf{1}\end{pmatrix}\,. \tag{2.15}$$

For future utility we also define

$$(\mathscr{T}_j)_{\vec{x}ak,\vec{y}bl} = \delta_{\vec{x}+\hat{\jmath},\vec{y}}\delta_{ab}\delta_{kl}\,, \quad k,l=0,\ldots,\tfrac{N_T}{2}-1\,. \tag{2.16}$$

We now make use of the block structure of the Dirac-Anderson Hamiltonian [see Eq. (2.13)], and of the fact that it anticommutes with the unitary matrix $\mathcal{Q} = \eta_4\Sigma_1$,[3] to simplify the study of the eigenvalue problem. The eigenvectors of $\mathcal{Q}$ are of the form

$$\psi_\pm[\varphi] = \frac{1}{\sqrt{2}}\begin{pmatrix}\varphi \\ \pm\eta_4\varphi\end{pmatrix}\,, \qquad \mathcal{Q}\psi_\pm[\varphi] = \pm\psi_\pm[\varphi]\,, \tag{2.17}$$

where φ are $\frac{N_T}{2}$-dimensional. One can easily show that

$$\Sigma_1\psi_\pm[\varphi] = \pm\eta_4\psi_\pm[\varphi]\,, \qquad \Sigma_3\psi_\pm[\varphi] = \psi_\mp[\varphi]\,, \qquad \mathcal{T}_j\psi_\pm[\varphi] = \psi_\mp[\mathscr{T}_j\varphi]\,. \tag{2.18}$$

[3] This is the analogue of the well-known anticommutation relation of the staggered operator with $\eta_5 \equiv (-1)^{\sum_\nu x_\nu}$.

Making use of this we find

$$\begin{aligned}\mathcal{H}\psi_\pm[\varphi] &= \psi_\mp[\mathscr{H}_\pm\varphi]\,,\\ \mathscr{H}_\pm &= \eta_4\mathscr{D} + \frac{1}{2i}\sum_j \eta_j\left[\mathscr{U}_j^{\mp}\mathscr{T}_j - \mathscr{T}_j^\dagger\mathscr{U}_j^{\pm\dagger}\right]\,,\end{aligned} \tag{2.19}$$

where the matrices

$$\mathscr{U}_j^{\pm} \equiv \mathscr{A}_j \pm \eta_4\mathscr{B}_j \tag{2.20}$$

are unitary, as a consequence of the unitarity of $\mathcal{V}_j$. One can also prove that $\det\mathcal{V}_j = \det(\mathscr{A}_j+\mathscr{B}_j)\det(\mathscr{A}_j-\mathscr{B}_j) = \det\mathscr{U}_j^+\det\mathscr{U}_j^-$. From the orthogonality of ψ_+ and ψ_- it follows that

$$(\psi_{s_1}[\varphi_k], \mathcal{H}\psi_{s_2}[\varphi_{k'}]) = \delta_{s_1,-s_2}(\varphi_k, \mathscr{H}_{s_2}\varphi_{k'})\,, \qquad s_{1,2} = \pm\,, \tag{2.21}$$

i.e., in the basis $\psi_\pm[\varphi_k]$, with $\{\varphi_k\}$ a basis of the $V\cdot\frac{N_T}{2}\cdot N_c$-dimensional space, one finds

$$[\mathcal{H}] = \begin{pmatrix} 0 & \mathscr{H}_- \\ \mathscr{H}_+ & 0\end{pmatrix}\,. \tag{2.22}$$

In order to determine the spectrum of $\mathcal{H}$, it is convenient to first diagonalise $\mathcal{H}^2$,

$$[\mathcal{H}^2] = \begin{pmatrix} \mathscr{H}_-\mathscr{H}_+ & 0 \\ 0 & \mathscr{H}_+\mathscr{H}_-\end{pmatrix} = \begin{pmatrix} \mathscr{H}_+^\dagger\mathscr{H}_+ & 0 \\ 0 & \mathscr{H}_+\mathscr{H}_+^\dagger\end{pmatrix}\,. \tag{2.23}$$

If $\mathscr{H}_+^\dagger\mathscr{H}_+\varphi_{\lambda^2} = \lambda^2\varphi_{\lambda^2}$, with $\lambda\neq 0$, then $(\mathscr{H}_+\mathscr{H}_+^\dagger)\mathscr{H}_+\varphi_{\lambda^2} = \mathscr{H}_+(\mathscr{H}_+^\dagger\mathscr{H}_+)\varphi_{\lambda^2} = \lambda^2\mathscr{H}_+\varphi_{\lambda^2}$, so that $\frac{\mathscr{H}_+}{\sqrt{\lambda^2}}\varphi_{\lambda^2}$ is a normalised eigenvector of $\mathscr{H}_+\mathscr{H}_+^\dagger$ with eigenvalue λ^2 if φ_{λ^2} is a normalised eigenvector of $\mathscr{H}_+^\dagger\mathscr{H}_+$. In conclusion, the eigenvectors of $\mathcal{H}^2$ are of the form $\psi_+[\varphi_{\lambda^2}]$ and $\psi_-[\frac{\mathscr{H}_+}{\sqrt{\lambda^2}}\varphi_{\lambda^2}]$.

In this paper we are interested in the localisation properties of the eigenmodes. As discussed in Ref. [23], a convenient measure of localisation is provided by the participation ratio $\mathrm{PR} = \mathrm{IPR}^{-1}/V$, where $V = L^3$ is the lattice volume and IPR is the inverse participation ratio, defined as

$$\mathrm{IPR} = \sum_{\vec{x}}\left(\sum_{a,k}|\psi_{ak}(\vec{x})|^2\right)^2\,. \tag{2.24}$$

With this definition, the knowledge of φ_{λ^2} is sufficient to determine the IPR: indeed,

$$\mathrm{IPR} = \sum_{\vec{x}}\left(\sum_{a,k}|\psi_{\pm ak}[\varphi(\vec{x})]|^2\right)^2 = \sum_{\vec{x}}\left(\sum_{a,\,0\le k<\frac{N_T}{2}}|\varphi_{ak}(\vec{x})|^2\right)^2\,. \tag{2.25}$$

For our purposes the problem is thus reduced to a $V\cdot\frac{N_T}{2}\cdot N_c$-dimensional one. This reduction is the analogue, in the present basis, of the well-known reduction of D^2_{stag} to the sum of two operators, each of which connects only even or odd sites, in the usual (coordinate) basis.

2.2 Dirac-Anderson Hamiltonian for $N_T = N_c = 2$

In the case $N_T = N_c = 2$ the problem simplifies considerably. In this case $\frac{N_T}{2} = 1$, so a single temporal-momentum component has to be considered, and $\mathscr{U}_j^{\pm}$ have the same dimensionality as $\hat{U}_j$. We have

$$\mathscr{D} = \cos\frac{\phi}{2}\mathbf{1}_{\rm c}\,, \tag{2.26}$$

where $\cos\frac{\phi}{2} = \mathrm{diag}(\cos\frac{\phi_{\vec{x}}}{2})$ is a diagonal matrix in position space, and $\mathbf{1}_{\rm c}$ is the identity in colour space. Moreover,

$$\mathscr{A}_j(\vec{x}) = \frac{1}{2}\left(\hat{U}_j(0,\vec{x}) + \hat{U}_j(1,\vec{x})\right)\,, \qquad \mathscr{B}_j(\vec{x}) = \frac{1}{2}\left(\hat{U}_j(0,\vec{x}) - \hat{U}_j(1,\vec{x})\right)\,, \tag{2.27}$$

and so

$$\mathscr{U}_j^{\pm}(\vec{x}) = \delta_{\pm}(\vec{x})\hat{U}_j(0,\vec{x}) + \delta_{\mp}(\vec{x})\hat{U}_j(1,\vec{x})\,, \tag{2.28}$$

where $\delta_{\pm}$ are the projectors on the even and the odd sublattices,

$$\delta_{\pm}(\vec{x}) = \frac{1 \pm \eta_4(\vec{x})}{2}\,, \qquad \delta_{\pm}^2 = \delta_{\pm}\,, \quad \delta_{\pm}\delta_{\mp} = 0\,. \tag{2.29}$$

Inverting these relations we find

$$\hat{U}_j(0,\vec{x}) = \delta_+(\vec{x})\mathscr{U}_j^+(\vec{x}) + \delta_-(\vec{x})\mathscr{U}_j^-(\vec{x})\,, \qquad \hat{U}_j(1,\vec{x}) = \delta_+(\vec{x})\mathscr{U}_j^-(\vec{x}) + \delta_-(\vec{x})\mathscr{U}_j^+(\vec{x})\,. \tag{2.30}$$

Notice that changing integration variables to $\mathscr{U}_j^{\pm}$ leaves the link integration measure unchanged. Let us work out in details the contribution ΔS_{ts} to the action. Since

$$W(\vec{x}) = \mathrm{diag}(e^{i\frac{\phi(\vec{x})}{2}}, e^{-i\frac{\phi(\vec{x})}{2}}) = \cos\frac{\phi(\vec{x})}{2}\mathbf{1}_{\rm c} + i\sin\frac{\phi(\vec{x})}{2}(\sigma_3)_{\rm c}\,, \tag{2.31}$$

after simple algebra one finds

$$\begin{aligned}\Delta S_{ts} = 2\sum_{j,\vec{x}} &\cos\frac{\phi(\vec{x})}{2}\cos\frac{\phi(\vec{x}+\hat{\jmath})}{2}\mathrm{Re}\,\mathrm{tr}\,[\mathscr{U}_j^+(\vec{x})\mathscr{U}_j^-(\vec{x})^\dagger] \\ &+ \sin\frac{\phi(\vec{x})}{2}\sin\frac{\phi(\vec{x}+\hat{\jmath})}{2}\mathrm{Re}\,\mathrm{tr}\,[\mathscr{U}_j^+(\vec{x})\sigma_3\mathscr{U}_j^-(\vec{x})^\dagger\sigma_3]\,.\end{aligned} \tag{2.32}$$

As for the Hamiltonian, it is entirely determined by

$$\mathscr{H}_{\pm} = \eta_4\cos\frac{\phi}{2} + \frac{1}{2i}\sum_{j=1}^{3}\eta_j\left[\mathscr{U}_j^{\mp}\mathscr{T}_j - \mathscr{T}_j^\dagger\mathscr{U}_j^{\pm\dagger}\right]\,. \tag{2.33}$$

2.3 Toy model

The toy model of Ref. [23] consists simply in replacing the Polyakov line phases and spatial links in the various terms appearing in Eq. (2.1) with suitable toy-model variables, and in choosing appropriate dynamics for these variables, intended to mimic that of the corresponding variables in QCD. In particular, the (diagonal) Polyakov lines $e^{i\phi_a(\vec{x})}$ are replaced by

complex spin variables $s^a_{\vec{x}} = e^{i\phi^a_{\vec{x}}}$, with dynamics governed by a suitable spin model. The only thing changing for the spatial links is the dynamics, which is still determined by a Wilson-like action (in the temporal diagonal gauge), obtained by dropping the contributions from spatial plaquettes, replacing the Polyakov lines with the diagonal matrices $\mathrm{diag}(s^a_{\vec{x}})$, and omitting the backreaction of the gauge links on the spins, i.e., treating the spins as external fields for the gauge links. The backreaction of fermions in the partition function is also omitted, i.e., the fermion determinant is dropped.

The simplifications of the Dirac-Anderson Hamiltonian discussed previously translate directly into simplifications for the toy model. Indeed, such simplifications are obtained by means of a gauge transformation for the link variables and of a change of basis for the Hamiltonian. In both cases, they amount to a unitary transformation of the Hamiltonian, which therefore leaves the spectrum unchanged. Moreover, since these transformations are local in space, they do not alter the localisation properties of the eigenmodes. The toy model obtained by making the substitutions discussed in the previous paragraph in the Hamiltonian [$\mathcal{H}$], Eq. (2.22), is thus unitarily equivalent to the one obtained by making the same substitutions in Eq. (2.1). In the case $N_c = N_T = 2$, which is the one studied numerically in Ref. [23], one can also make a change of variables for the links, as described in Eq. (2.30), leading to further simplifications.

All in all, the toy model for $N_c = N_T = 2$ of Ref. [23] can be equivalently formulated as follows. The toy model Hamiltonian reads

$$\mathcal{H}^{\mathrm{toy}} = \begin{pmatrix} 0 & \mathscr{H}^{\mathrm{toy}}_- \\ \mathscr{H}^{\mathrm{toy}}_+ & 0 \end{pmatrix}, \quad \mathscr{H}^{\mathrm{toy}}_\pm = \eta_4 \cos\frac{\phi}{2} + \frac{1}{2i}\sum_j \eta_j \left[\mathscr{U}_j^{\mp}\mathscr{T}_j - \mathscr{T}_j^\dagger \mathscr{U}_j^{\pm\dagger}\right], \tag{2.34}$$

where it is understood that all variables are now the toy-model variables, e.g., $\cos\frac{\phi}{2} = \mathrm{diag}(\frac{\cos\phi_{\vec{x}}}{2})$. The dynamics of the spin phases $\phi_{\vec{x}} \in [-\pi, \pi)$ is governed by the spin-model Hamiltonian

$$\beta H_{\mathrm{noise}} = -\beta \sum_{\vec{x},j} \cos(\phi_{\vec{x}+\hat{\jmath}} - \phi_{\vec{x}}) - h \sum_{\vec{x}} \cos(2\phi_{\vec{x}}), \tag{2.35}$$

as in Ref. [23]. Here β is the inverse temperature of the spin model, and h is a coupling which breaks the U(1) symmetry of the first term down to $\mathbb{Z}_2$. The dynamics of the toy-model link variables $\mathscr{U}_j^{\pm}(\vec{x}) \in \mathrm{SU}(2)$ is governed by the action

$$\begin{aligned} S_u = 2\hat{\beta} \sum_{j,\vec{x}} \cos\frac{\phi_{\vec{x}}}{2} \cos\frac{\phi_{\vec{x}+\hat{\jmath}}}{2} \mathrm{Re}\,\mathrm{tr}\,[\mathscr{U}_j^+(\vec{x})\mathscr{U}_j^-(\vec{x})^\dagger] \\ + \sin\frac{\phi_{\vec{x}}}{2} \sin\frac{\phi_{\vec{x}+\hat{\jmath}}}{2} \mathrm{Re}\,\mathrm{tr}\,[\mathscr{U}_j^+(\vec{x})\sigma_3\mathscr{U}_j^-(\vec{x})^\dagger\sigma_3], \end{aligned} \tag{2.36}$$

where $\hat{\beta}$ plays the role of gauge coupling. Expectation values are defined as follows:

$$\langle \mathcal{O} \rangle = \frac{\int D\phi\, e^{-\beta H_{\mathrm{noise}}[\phi]} \left[\frac{\int D\mathscr{U}\, e^{-S_u[\phi,\mathscr{U}]}\mathcal{O}[\phi,\mathscr{U}]}{\int D\mathscr{U}\, e^{-S_u[\phi,\mathscr{U}]}}\right]}{\int D\phi\, e^{-\beta H_{\mathrm{noise}}[\phi]}}, \tag{2.37}$$

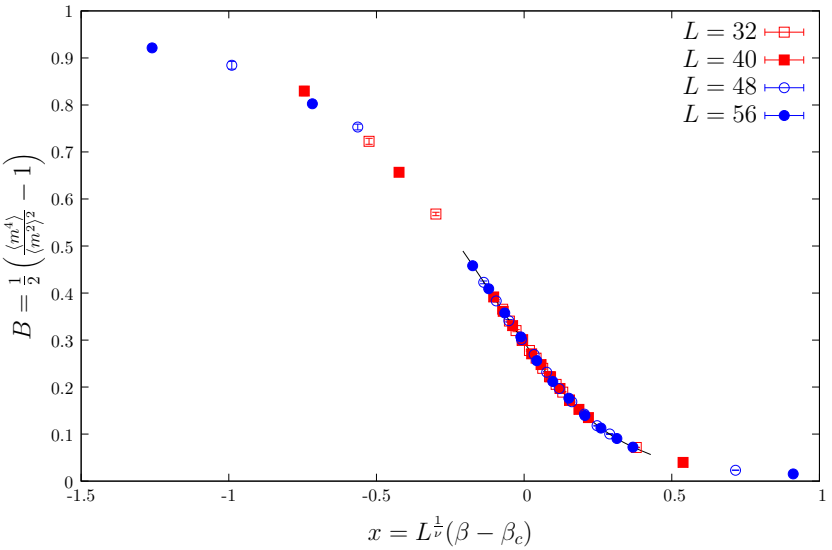

Figure 1. Finite size scaling analysis for the Binder cumulant B. The scaling function is also shown (solid line).

where $\int D\phi = \prod_{\vec{x}} \int_{-\pi}^{+\pi} d\phi_{\vec{x}}$ and $D\mathscr{U} = \prod_{\vec{x},j} d\mathscr{U}_j^+(\vec{x}) d\mathscr{U}_j^-(\vec{x})$, with $d\mathscr{U}_j^{\pm}(\vec{x})$ the Haar measure. Notice the absence of backreaction of the gauge links on the spins.

The features that have been stripped from QCD in order to build the toy model are those deemed irrelevant for the qualitative behaviour of eigenvalues and eigenvectors of the Dirac operator. What has been kept is the presence of order in the configuration of the variables governing the diagonal noise of the Hamiltonian, and the correlations that such order induces on the spatial links. The choice $N_T = 2$ in lattice QCD is certainly not likely to lead to good quantitative results, but is nevertheless a legitimate (and indeed the simplest) choice one can make to build a toy model which resembles QCD (or rather SU(N_c) pure gauge theory) qualitatively. The results of Ref. [23] show that the toy model described above is indeed capable of reproducing the important features of the spectrum and of the eigenmodes, both in the ordered and in the disordered phase.

3 Numerical results

In this section we report the results of a numerical study of the toy model defined by Eqs. (2.34)–(2.37) in the vicinity of the phase transition in the underlying spin model. Numerical simulations near a critical point are hampered by critical slowing down, but this problem can be overcome using a suitable cluster algorithm. This is discussed in subsection 3.1, where we report the results of a detailed finite-size-scaling study of the spin model Eq. (2.35), aimed at determining the critical coupling and the universality class of the transition.

We then proceed to study in our toy model the issues of localisation and chiral transition, the latter understood here as a singularity in the spectral density at the origin. The most

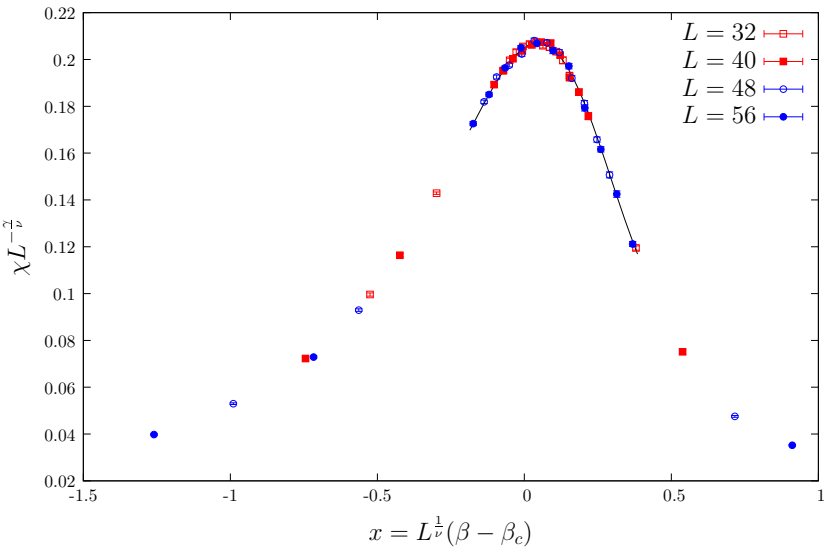

Figure 2. Finite size scaling analysis for the magnetic susceptibility χ. The scaling function is also shown (solid line).

effective observables in pinning down the coupling(s) at which localisation appears and/or where a chiral transition takes place, are respectively the participation ratio of the lowest eigenmode and the corresponding level spacing. This is discussed in subsection 3.2, where we also report the results of our numerical study.

3.1 Finite-size-scaling study of the spin model

We begin by studying the spin model on its own near the critical point. The formulation of a cluster algorithm to this end is made easier by noticing that Eq. (2.35) can be recast as

$$\beta H_{\text{noise}} = -\beta \sum_{\vec{x},j} \hat{n}_{\vec{x}} \cdot \hat{n}_{\vec{x}+\hat{j}} - h \sum_{\vec{x}} \left[2 \left(\hat{n}_{\vec{x}} \cdot \hat{n}_* \right)^2 - 1 \right] , \tag{3.1}$$

where

$$\hat{n}_{\vec{x}} = \begin{pmatrix} \cos \phi_{\vec{x}} \\ \sin \phi_{\vec{x}} \end{pmatrix} , \qquad \hat{n}_* = \begin{pmatrix} 1 \\ 0 \end{pmatrix} . \tag{3.2}$$

Near the transition $\hat{n}_{\vec{x}}$ tends to be aligned to $\pm\hat{n}_*$, forming large clusters of like-oriented spins, and this leads to long autocorrelation times in the simulation history. To overcome critical slowing down we thus employed a Wolff-type cluster algorithm [25] consisting of the following steps.

1. Given a spin configuration, we pick a site at random and build a cluster, adjoining nearby sites $\vec{x}$ and $\vec{x} \pm \hat{j}$ with probability

$$P(\vec{x}, \vec{x} \pm \hat{j}) = 1 - e^{-2\beta |\hat{n}_{\vec{x}} \cdot \hat{n}_*| |\hat{n}_{\vec{x}\pm\hat{j}} \cdot \hat{n}_*|} = 1 - e^{-2\beta |\cos \phi_{\vec{x}}| |\cos \phi_{\vec{x}+\hat{j}}|} . \tag{3.3}$$

	our model	3D Ising model
β_c	0.3023210(38)	—
B^*	0.2952(13)	0.3022(13)
ν	0.6393(84)	0.6301(8)
γ	1.2660(26)	1.237(2)

Table 1. Critical point, critical Binder cumulant and critical exponents of our spin model, and of the 3D Ising model [26].

2. Once the cluster is built, we flip $\hat{n}_{\vec{x}} \to -\hat{n}_{\vec{x}}$, i.e., we send $\phi_{\vec{x}} \to \pi \operatorname{sgn}(\phi_{\vec{x}}) - \phi_{\vec{x}}$, for all sites $\vec{x}$ in the cluster.

This algorithm is easily shown to respect detailed balance, but it obviously fails at being ergodic. For this reason, we paired it with a standard Metropolis algorithm, which restores ergodicity.

We studied the model as a function of β keeping the symmetry-breaking term fixed at $h = 1.0$. Defining the magnetisation of the system as

$$m = \sum_{\vec{x}} \operatorname{Re} s_{\vec{x}} = \sum_{\vec{x}} \cos \phi_{\vec{x}} \,, \tag{3.4}$$

we measured the susceptibility and the fourth-order Binder cumulant:

$$\chi = \frac{1}{V} \left(\langle m^2 \rangle - \langle m \rangle^2 \right) \,, \qquad B = \frac{1}{2} \left(\frac{\langle m^4 \rangle}{\langle m^2 \rangle^2} - 1 \right) \,. \tag{3.5}$$

Our definition of B is such that $B \to 1$ in the disordered phase and $B \to 0$ in the ordered phase. Near the critical point, β_c, the expected behaviour of B and χ is

$$\begin{aligned} B(\beta) &\approx f\left(L^{\frac{1}{\nu}} (\beta - \beta_c) \right) \,, \\ \chi(\beta) &\approx L^{\frac{\gamma}{\nu}} g\left(L^{\frac{1}{\nu}} (\beta - \beta_c) \right) \,. \end{aligned} \tag{3.6}$$

We thus fitted the numerical data in the range $\beta \in [0.302, 0.303]$ and for the available volumes with the functional forms of Eq. (3.6), using polynomial approximations of f and g of increasing order, and assessing the error by means of constrained fit techniques [24]. Our results for the critical point, the critical exponents ν and γ, and the critical Binder cumulant B^* are reported in Tab. 1. These values give an excellent "collapse" of the data points on a single, volume-independent curve, as shown in Figs. 1 and 2. For comparison, in Tab. 1 we report also the results of Blöte *et al.* for the 3D Ising model [26]. The tension in the results for B^* and γ is probably due to the fact that we are not including the effect of irrelevant couplings in our analysis. Nevertheless, our results strongly support the fact that the transition observed in our model belongs to the 3D Ising universality class.

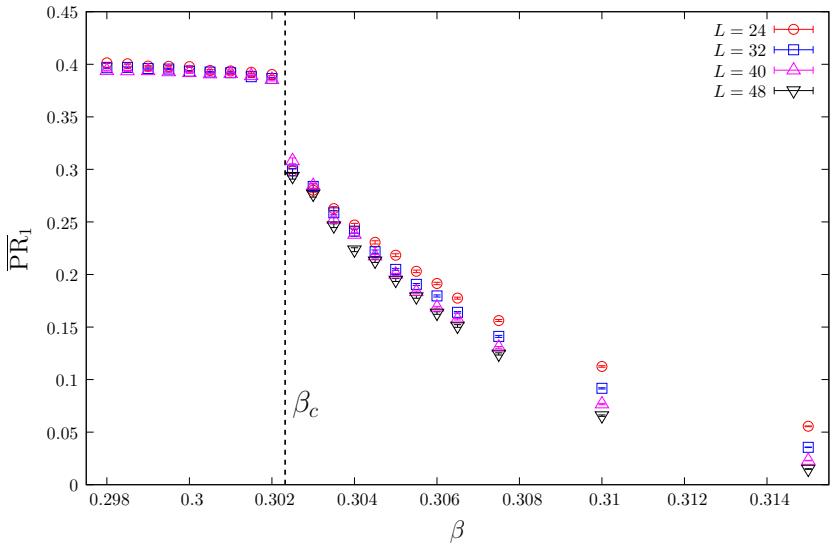

Figure 3. Average participation ratio of the first eigenmode as a function of β.

3.2 Onset of localisation and chiral transition in the toy model

Let us discuss first the issue of localisation. The simplest way to check for localisation is to compute the so-called "participation ratio", PR_n, of the n-th eigenmode, ψ_n, defined as

$$\mathrm{PR}_n = \frac{1}{V}\mathrm{IPR}_n^{-1} = \frac{1}{V}\left[\sum_{\vec{x}} |\psi_n^\dagger(\vec{x})\psi_n(\vec{x})|^2\right]^{-1} , \tag{3.7}$$

where IPR stands for "inverse participation ratio", and $\psi_n^\dagger\psi_n = \sum_{a,k}(\psi_n)_{ak}^*(\psi_n)_{ak}$ stands for summation over the colour and temporal-momentum degrees of freedom. Here $V = L^3$ is the spatial volume. If the n-th mode is localised, then the average of PR_n over configurations, which we denote by $\overline{\mathrm{PR}_n}$, is expected to vanish in the large-volume limit. On the other hand, for delocalised modes this quantity becomes constant at large volume. We already know from Ref. [23] that localised modes appear first near the origin, so in order to check whether there are localised modes or not, it is sufficient to compute the participation ratio of the first eigenmode, and check how it changes with the volume. In Fig. 3 we show the average participation ratio of the first eigenmode, $\overline{\mathrm{PR}_1}$, as a function of β for different system sizes, namely $L = 24, 32, 40$ and, in the ordered phase only, also $L = 48$. The localisation properties of the lowest mode are clear below β_c and well above it. In the disordered phase the lowest mode is delocalised, while it is localised deep in the ordered phase. Starting form large β and going down towards β_c the scaling with V becomes slower, and very close to β_c the participation ratio actually grows up to $L = 40$. Nevertheless, $\overline{\mathrm{PR}_1}$ displays a jump at β_c, and the largest volume always gives the smallest participation ratio. We take these findings as an indication that also right above β_c the lowest eigenmode has the tendency to localise. This tendency is, however, hampered by the fact that the typical localisation length

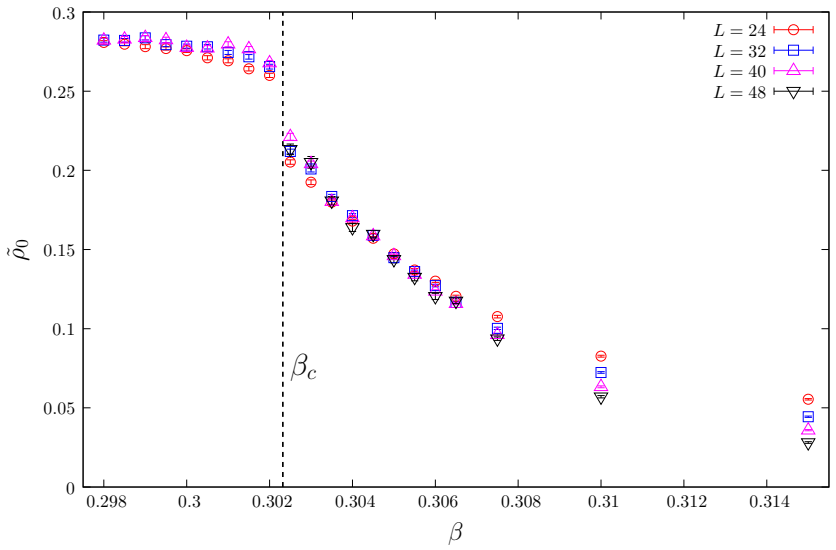

Figure 4. The quantity $\tilde{\rho}_0$, defined in Eq. (3.8).

is bigger than or comparable to the system sizes under consideration. As a consequence, the would-be (lowest) localised eigenmode is effectively delocalised on the whole lattice, thus having a strong overlap with the extended modes, and therefore mixing easily with them under fluctuations of the spins and of the gauge fields. Moreover, we expect its participation ratio to grow until the system is big enough to accommodate a localised mode, whereas it will start to decrease for even larger sizes. In conclusion, we expect that for sufficiently large systems the lowest eigenmode is localised as soon as $\beta > \beta_c$. The closer one is to β_c, the larger the system has to be for localisation to be fully visible.

Let us consider next the issue of the chiral transition. In principle (and by definition), this issue should be studied by analysing the spectral density near the origin. In practice, however, this is very hard in the vicinity of the critical point, and could be done reliably only using high statistics and large volumes, in order to sample properly the near-zero spectral region. Rather than attempting a (difficult) direct measurement, we relied upon the following relation:

$$\tilde{\rho}_0 \equiv \frac{1}{V\langle\lambda_2 - \lambda_1\rangle} \underset{V\to\infty}{\to} \frac{\rho(0)}{V}\,, \tag{3.8}$$

which is based on the following argument. In the large-volume limit, the spectral density at the origin is equal to the inverse of the average level spacing in the near-zero spectral region. In the same limit, and for fixed j, one has for the eigenvalues of the Dirac operator (and thus for those of our toy-model Hamiltonian) that $\lambda_j \to 0$. Eq. (3.8) then follows. This applies to any fixed j, but of course one expects that for too large j the finite-size effects would completely obscure the limit (however, see below for some numerical results for $j = 2, 3$). In Fig. 4 we show $\tilde{\rho}_0$ as a function of β for the available system sizes. It is clear that below β_c this quantity tends to a finite constant as the volume is increased. For our largest values

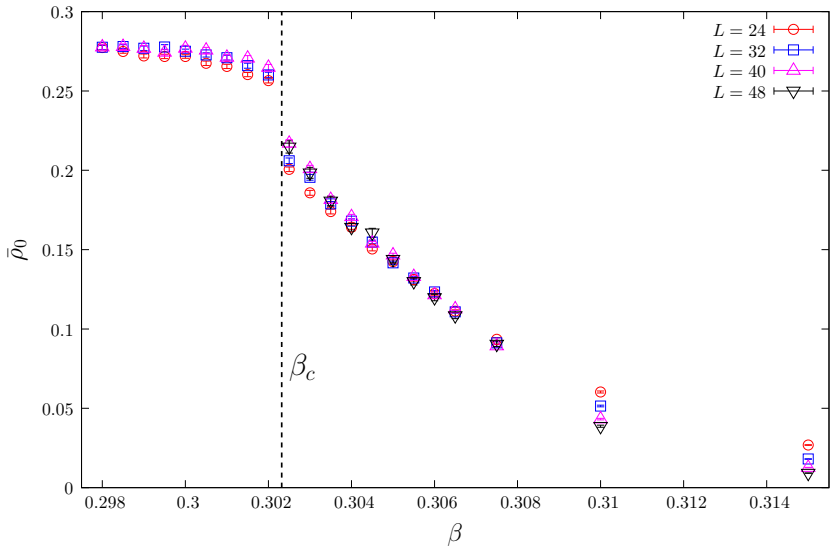

Figure 5. The quantity $\bar{\rho}_0$ defined in Eq. (3.11).

of β above β_c, on the contrary, there is a clear tendency for $\tilde{\rho}_0$ to vanish as $V \to \infty$. The region which is most difficult to understand is right above β_c. There $\tilde{\rho}_0$ apparently tends to a finite constant, different from the one right below β_c. Although it is possible that there are two jumps in $\tilde{\rho}_0$, one at β_c and another at some higher value of β where $\tilde{\rho}_0$ jumps to zero, we think that there is a more plausible explanation for this behaviour. In fact, as we have already mentioned above, the relative smallness of the system that causes the lowest mode to be effectively delocalised, is also responsible for its mixing with nearby modes under fluctuations of spins and link variables. The behaviour of the lowest mode is thus expected to be similar in all respects to what is found in the disordered phase, and more generally the low end of the spectrum is expected to look like in the disordered phase. This includes a nonzero spectral density near the origin. It is likely that for large enough systems, $\tilde{\rho}_0$ will start to show a nontrivial scaling with V, indicating the vanishing of the spectral density at the origin in the thermodynamic limit. In any case, whether $\rho(0)$ vanishes right above β_c or not, it is clear that at β_c it displays a singularity. This indicates that the system has a chiral transition at β_c.

An alternative way of determining $\rho(0)$ is based on its relation with the expectation value of the lowest eigenvalue, $\langle \lambda_1 \rangle$. In the disordered phase, where $\rho(0) \neq 0$, the probability distribution of the lowest eigenvalue is expected to be described by the appropriate ensemble of chRMT. In the case at hand, this should be the symplectic ensemble for the quenched theory in the trivial topological sector, and so [27–31]

$$p_1(z) = \sqrt{\frac{\pi}{2}} z^{\frac{3}{2}} I_{\frac{3}{2}}(z) e^{-\frac{z^2}{2}} , \tag{3.9}$$

where $z = \lambda_1 \pi \rho(0)$. From this one obtains the appropriate proportionality factor between

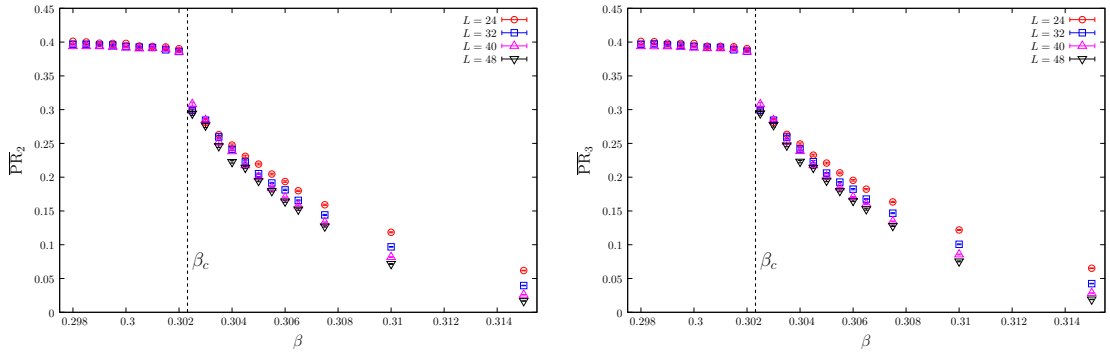

Figure 6. Average participation ratio of the second and third eigenmode as a function of β.

$\langle\lambda_1\rangle$ and $\rho(0)$, namely

$$\rho(0) = \sqrt{\frac{e}{2\pi}}\,\frac{1}{\langle\lambda_1\rangle}\,. \tag{3.10}$$

For localised modes one expects instead that the corresponding eigenvalues obey Poisson statistics. In this case, assuming a power-law behaviour $\rho(\lambda) = CV\lambda^\alpha$ for the spectral density near the origin, one finds [12] that $\langle\lambda_1\rangle \sim V^{-\frac{1}{1+\alpha}}$, and in particular $\rho(0) = \frac{1}{\langle\lambda_1\rangle}$ for $\alpha = 0$. Our results for $\bar\rho_0$,

$$\bar\rho_0 \equiv \sqrt{\frac{e}{2\pi}}\,\frac{1}{V\langle\lambda_1\rangle}\,, \tag{3.11}$$

are shown in Fig. 5. Comparing this with Fig. 4 we see that the chRMT result works well below β_c, while it works less and less well as β increases above β_c. In particular, for large β one has that $\bar\rho_0$ tends to vanish as the volume is increased, signalling a vanishing spectral density at the origin. As before, the region right above β_c is the one where things are less clear. A nonvanishing $\rho(0)$ accompanied by localisation of the lowest modes right above β_c should yield a $\bar\rho_0$ appreciably smaller than $\rho(0)$, and so of $\tilde\rho_0$, while the two quantities compare well. This is most likely another consequence of the smallness of the system size compared to what would be required to properly investigate the region near the critical point. In fact, the effective delocalisation and easy mixing of the lowest mode mentioned above leads to correlations building up among eigenvalues, thus leading to a chRMT-like statistical behaviour, which should go over to Poisson behaviour as the system size increases.

For completeness, we conclude this section by showing our numerical results concerning the second and third lowest eigenmodes. In Fig. 6 we show the average participation ratios $\overline{\mathrm{PR}_2}$ and $\overline{\mathrm{PR}_3}$. The situation is entirely analogous to that encountered when studying the lowest mode, with similar finite-size effects near the transition which slow down the localisation of these modes. In Fig. 7 we show the quantities

$$\tilde\rho_0' \equiv \frac{1}{V\langle\lambda_3 - \lambda_2\rangle}\,, \qquad \tilde\rho_0'' \equiv \frac{1}{V\langle\lambda_4 - \lambda_3\rangle}\,, \tag{3.12}$$

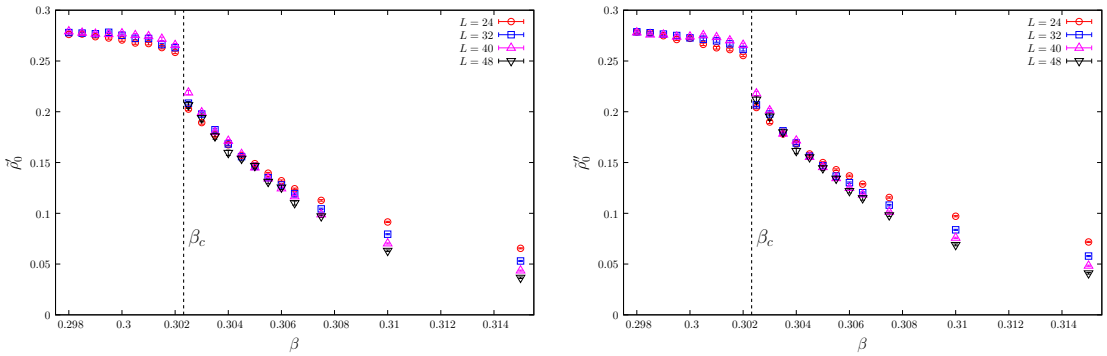

Figure 7. The quantities $\tilde{\rho}_0'$ and $\tilde{\rho}_0''$, defined in Eq. (3.12).

which in the large volume limit should also approach $\frac{\rho(0)}{V}$. In this case the volume scaling is somewhat more clear, with the tendency to go to zero as V is increased showing up for lower values of β. These results clearly do not change the conclusions discussed above.

4 Conclusions and outlook

There are by now several hints at a close connection between the deconfining and chiral transitions and localisation of the lowest eigenmodes of the Dirac operator. In this paper we have further studied the toy model of Ref. [23], which mimics the effects of the ordering of Polyakov loops in QCD, i.e., deconfinement, on the spectral density of the low Dirac eigenmodes and the corresponding localisation properties. In particular, we have focussed on the region near the magnetic transition of the underlying spin model, which corresponds to deconfinement in a gauge theory. We have then studied numerically the localisation properties of the lowest eigenmode, and the spectral density at the origin. Our findings are consistent with a chiral transition taking place in correspondence with the magnetic transition, accompanied by the appearance of localised modes. This further supports our expectation that deconfinement plays a major role in the chiral transition and in the localisation of the low Dirac modes observed in QCD.

There are, however, several aspects that deserve further studies. The presence of a chiral transition in our toy model when the spins get ordered is quite clear, since the spectral density at the origin shows a jump there. However, it is not clear yet if such a jump is from the finite value of $\rho(0)$ in the disordered phase to zero in the ordered phase, or to a different finite value. Although the latter possibility seems unlikely, nevertheless the presence of strong finite-size effects makes it difficult to extrapolate to the infinite-volume limit. The origin of such effects lies in the fact that although the lowest modes would like to be localised, their typical localisation length is bigger than the system sizes at our disposal. This makes those modes effectively delocalised on our finite lattices, and so easily mixed by fluctuations with other nearby modes. In turn, this is probably responsible for a smaller typical level spacing between the first two eigenvalues, from which the spectral density was extracted. Consequently, we

are probably overestimating $\rho(0)$. Moreover, the lowest eigenmode correlates with the nearby modes, which results in statistical properties closer to those predicted by chRMT than to those expected for localised modes, which should obey Poisson statistics. In order to overcome these problems, and unveil the true nature of the lowest modes, bigger lattices should be employed.

This situation should be contrasted to that found with unimproved staggered fermions on coarse lattices [18]. In that case the coincindence of deconfinement, chiral transition and appearance of localised modes is more clean-cut. A possible explanation of the difference lies in the different nature of the deconfining transition in that system, which is a first-order transition, and the magnetic transition in our toy model, which is a second-order phase transition of the 3D Ising universality class. In the case at hand, the presence of a huge correlation length near the critical point, and at the same time the fact that the magnetisation is very small there, makes it more difficult for the low modes to properly localise. As we said above, this is expected to be the source of the large finite-size effects observed in our determination of $\rho(0)$.

Despite these difficulties, we think that our results confirm those of previous studies in other models, in showing that deconfinement, chiral transition and localisation are closely tied to each other. There are several possible extensions of the present study. One obvious possibility is to consider our toy model for gauge group SU(3), thus making it closer to QCD. This involves a different spin model to mimic the behaviour of the Polyakov lines than the one employed here (see Ref. [23] for details). A more interesting possibility is to extend the toy model to the case of adjoint fermions: this could help in understanding why for adjoint fermions deconfinement and chiral restoration take place at different temperatures [7].

References

[1] Y. Aoki, Z. Fodor, S. D. Katz and K. K. Szabó, Jour. High Energy Phys. **01** (2006) 089 [hep-lat/0510084].

[2] S. Borsányi, G. Endrődi, Z. Fodor, A. Jakovác, S. D. Katz, S. Krieg, C. Ratti and K. K. Szabó, Jour. High Energy Phys. **11** (2010) 077 [arXiv:1007.2580 [hep-lat]].

[3] J. B. Kogut, M. Stone, H. W. Wyld, W. R. Gibbs, J. Shigemitsu, S. H. Shenker and D. K. Sinclair, Phys. Rev. Lett. **50** (1983) 393.

[4] F. Karsch, E. Laermann and C. Schmidt, Phys. Lett. B **520** (2001) 41 [hep-lat/0107020].

[5] P. de Forcrand and O. Philipsen, Nucl. Phys. B **673** (2003) 170 doi:10.1016/j.nuclphysb.2003.09.005 [hep-lat/0307020].

[6] P. de Forcrand and O. Philipsen, Jour. High Energy Phys. **11** (2008) 012 [arXiv:0808.1096 [hep-lat]].

[7] F. Karsch and M. Lütgemeier, Nucl. Phys. B **550** (1999) 449 [hep-lat/9812023].

[8] J. J. M. Verbaarschot and T. Wettig, Ann. Rev. Nucl. Part. Sci. **50** (2000) 343 [hep-ph/0003017].

[9] P. de Forcrand, AIP Conf. Proc. **892** (2007) 29 [hep-lat/0611034].

[10] A. M. García-García and J. C. Osborn, Nucl. Phys. A **770** (2006) 141 [hep-lat/0512025].

[11] A. M. García-García and J. C. Osborn, Phys. Rev. D **75** (2007) 034503 [hep-lat/0611019].

[12] T. G. Kovács, Phys. Rev. Lett. **104** (2010) 031601 [arXiv:0906.5373 [hep-lat]].

[13] T. G. Kovács and F. Pittler, Phys. Rev. Lett. **105** (2010) 192001 [arXiv:1006.1205 [hep-lat]].

[14] F. Bruckmann, T. G. Kovács and S. Schierenberg, Phys. Rev. D **84** (2011) 034505 [arXiv:1105.5336 [hep-lat]].

[15] T. G. Kovács and F. Pittler, Phys. Rev. D **86** (2012) 114515 [arXiv:1208.3475 [hep-lat]].

[16] M. Giordano, T. G. Kovács and F. Pittler, PoS LATTICE **2013** (2013) 212 [arXiv:1311.1770 [hep-lat]].

[17] M. Giordano, T. G. Kovács and F. Pittler, Phys. Rev. Lett. **112** (2014) 102002 [arXiv:1312.1179 [hep-lat]].

[18] M. Giordano, T. G. Kovács, S. D. Katz and F. Pittler, arXiv:1611.03284 [hep-lat].

[19] M. Giordano, T. G. Kovács and F. Pittler, Int. J. Mod. Phys. A **29** (2014) 1445005. [arXiv:1409.5210 [hep-lat]].

[20] G. Cossu and S. Hashimoto, Jour. High Energy Phys. **06** (2006) 056 [arXiv:1604.00768 [hep-lat]].

[21] A. Tomiya, G. Cossu, S. Aoki, H. Fukaya, S. Hashimoto, T. Kaneko and J. Noaki, arXiv:1612.01908 [hep-lat].

[22] M. Giordano, T. G. Kovács and F. Pittler, Jour. High Energy Phys. **04** (2015) 112 [arXiv:1502.02532 [hep-lat]].

[23] M. Giordano, T. G. Kovács and F. Pittler, Jour. High Energy Phys. **06** (2016) 007 [arXiv:1603.09548 [hep-lat]].

[24] G. P. Lepage, B. Clark, C. T. H. Davies, K. Hornbostel, P. B. Mackenzie, C. Morningstar and H. Trottier, Nucl. Phys. Proc. Suppl. **106** (2002) 12. [hep-lat/0110175].

[25] U. Wolff, Phys. Rev. Lett. **62** (1989) 361.

[26] H. W. J. Blöte, E. Luijten and J. R. Heringa, J. Phys. A: Math. Gen. **28** (1995) 6289 [arXiv:cond-mat/9509016].

[27] P. J. Forrester, Nucl. Phys. B **402** (1993) 709.

[28] J. Kaneko, SIAM J. Math. Anal. **24** (1993) 1086.

[29] M. E. Berbenni-Bitsch, S. Meyer and T. Wettig, Phys. Rev. D **58** (1998) 071502 [hep-lat/9804030].

[30] S. M. Nishigaki, P. H. Damgaard and T. Wettig, Phys. Rev. D **58** (1998) 087704 [hep-th/9803007].

[31] S. M. Nishigaki, PoS LATTICE **2015** (2016) 057 [arXiv:1606.00276 [hep-lat]].